Letter

Intrinsic Mobility of Low-Density Electrons in Photoexcited Diamond

K. Konishi,[1] I. Akimoto,[2] H. Matsuoka,[3] J. Isberg,[4] and N. Naka[1,*]

[1] *Department of Physics, Kyoto University, Kitashirakawa-Oiwake-cho, Sakyo-ku, Kyoto 606-8502, Japan*
[2] *Department of Materials Science and Chemistry, Wakayama University, Sakaedani 930, Wakayama 640-8510, Japan*
[3] *Graduate School of Science, Osaka City University, Sugimoto 3-3-138, Sumiyoshi-ku, Osaka 558-8585, Japan*
[4] *Department of Electrical Engineering, Uppsala University, Box 65, S-751 03 Uppsala, Sweden*

(Received 21 September 2021; revised 25 February 2022; accepted 28 February 2022; published 23 March 2022)

Extending the limit of charge-carrier mobility in semiconductors has been a long-standing pursuit in material science and its applications. Herein, we investigate the electron mobility via cyclotron resonance in undoped diamond under continuous-wave photoexcitation, whereby the density of charge carriers can be reduced to 10^8 cm^{-3} or 1/10 of the previous detection limit [K. Konishi *et al.*, Appl. Phys. Lett. **117**, 212102 (2020)]. For low-density electrons, which obviate the effects of carrier-carrier scattering as a broadening mechanism, we observe an extraordinarily narrow cyclotron resonance spectrum. After correcting for the microwave power broadening, the highest intrinsic mobility value of 100×10^6 cm^2 V^{-1} s^{-1} is obtained at 3 K, which is a 16-fold increase of the mobility compared with the previous record in diamond. Our result is beneficial for the design and application of diamond radiation detectors implemented for their practical use at cryogenic temperatures.

DOI: 10.1103/PhysRevApplied.17.L031001

The mobility, diffusion, and lifetime of charge carriers govern semiconductor device performance. However, the applicable measurement principles pose several challenges even today [1], as exemplified by the revolutionary demonstration of the carrier-resolved photo-Hall effect [2] as an extension of the standard Hall measurement. The cyclotron resonance (CR) method is another powerful tool for determining the drift mobility of charge carriers [3] using a microwave probe without electrical contact. The mobility is obtained as the inverse of half the width of a CR line. With the progress of ultrafast laser technology, the probe frequency has been extended to a wide band spanning 30–330 GHz [4,5], and a magnetic field strength as high as 560 T has been employed [6]. This method has been applied to explore intriguing physical phenomena, such as screening effects [7] and coherent CR motion [8] in two-dimensional electron gases (2DEGs) in heterostructures, bulk states of Dirac and Weyl semimetals [9], relativistic fermions in the surface states of topological insulators [10], and quantum limit CR in atomically thin conductors [6].

We have explored the transport properties of photoexcited charge carriers in a variety of semiconductors [11–13] by developing a time-resolved CR (TRCR) method. Extremely high mobility has been found in intrinsic diamond [14]; however, the highest value was limited not by residual impurities [15] but by an unknown effect, possibly related to carrier-carrier interactions [16]. For photoexcitation of diamond with a large energy gap (5.5 eV), pulsed laser light has been used [14,17,18], which generates charge carriers at a density of 10^9–10^{11} cm^{-3} in a sea of excitons, i.e., Coulomb-bound electron-hole pairs [see Fig. 1(a)]. For such relatively high-density systems, carrier-carrier scattering can hinder the determination of intrinsic carrier mobility. Here, the term "intrinsic" refers to phonon scattering, while extrinsic mechanisms include scattering by other carriers, impurities, and dislocations.

In this study, we create electrons at a sufficiently low density under continuous-wave (CW) photoexcitation instead of pulsed laser light [Fig. 1(b)]; therefore, carrier-carrier scattering is irrelevant. Such a low density of electrons cannot be probed in our pulsed excitation regime because the pulse-to-pulse intervals (100 ms) of the tunable deep-ultraviolet laser are significantly longer than the carrier lifetimes (< 2 μs). We observe an extremely narrow CR spectrum indicating a high mobility value of 36×10^6 cm^2 V^{-1} s^{-1}. After correcting for the microwave power broadening, we further derive the intrinsic mobility at 100×10^6 cm^2 V^{-1} s^{-1}, which is governed by inelastic acoustic-phonon scattering. Because conventional Hall effect measurements are not possible for low-temperature diamond without thermal carrier activation and the time-of-flight (TOF) method causes carrier heating by the applied electric field, our technical development

*naka@scphys.kyoto-u.ac.jp

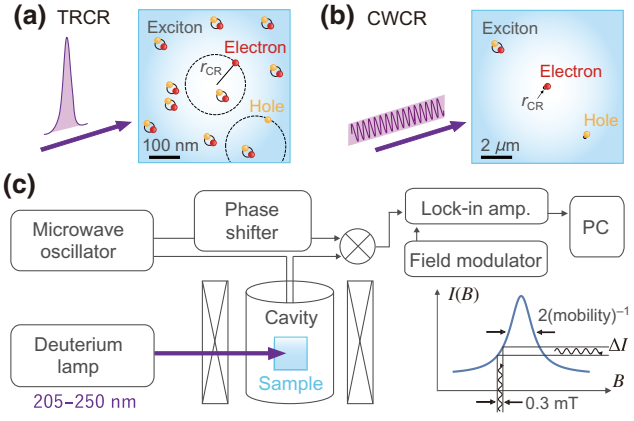

FIG. 1. Schematics of charge carriers with cyclotron radius r_{CR} in diamond under (a) pulsed and (b) CW photoexcitation. Note the exaggerated particle size and the different length scales in (a) and (b). (c) Experimental setup of CWCR.

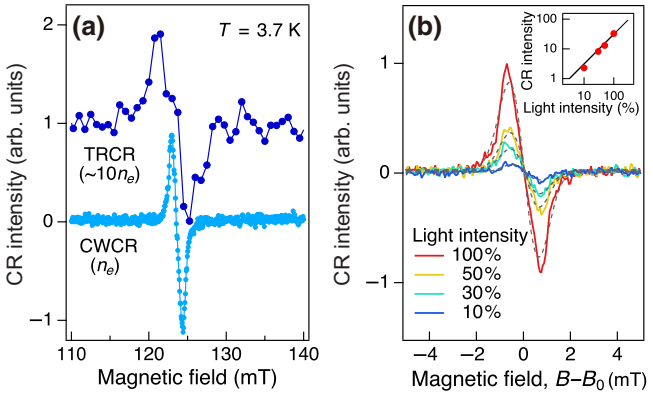

FIG. 2. (a) Differential spectra of TRCR and CWCR in Sample 3 at 3.7 K and a microwave power of $P = 250$ nW ($Q = 10^4$). (b) CWCR spectra measured in Sample 2 at 3.0 K at different light intensities. Full lines are experimental data and dashed lines represent Gaussian function fits. The horizontal axis indicates difference in magnetic field from the resonance, $B - B_0$. The inset shows integrated signal intensity as a function of incident light intensity.

and findings provide valuable information on *ideal* carrier transport properties, which impact the design of diamond radiation detectors used at cryogenic temperatures [19].

Three single-crystal chemical-vapor-deposition diamonds (Samples 1, 2, and 3, with dimensions of a few square millimeters and thickness of approximately 0.5 mm) of the highest possible elemental purity are supplied by Element Six. Samples 1 and 3 are custom grown, while Sample 2 is a commercially available electronic-grade sample [18]. The differences in the dislocation densities [20] are detailed in Supplemental Material S1 [21]. We use CW light from a deuterium lamp for photoexcitation [Fig. 1(c)]. The wavelengths in the range of 205–250 nm are selected using harmonic separators (Ekspla Ltd), so that charge carriers are more efficiently excited [22] than those using monochromatic light at 225 nm for the resonant exciton creation [11]. The power of the incident light is typically 400 μW outside the cryostat. The electron density is estimated to be $n_e < 1 \times 10^9$ cm^{-3} by considering the incident power, absorption coefficient, and diffusion length (Supplemental Material S2 [21]) [23–25]. The sample is placed in a dielectric cavity resonator (Bruker, MD5W1) at a microwave frequency of $f = 9.6$ GHz and cooled in a continuous-flow cryostat [14]. To improve the detection sensitivity, the magnetic field is modulated by ± 0.15 mT at 100 kHz [26], and the differential signal of microwave absorption is measured via lock-in detection.

We focus on the electron resonance signal at $B_0 = 123$ mT, for which the effective mass m_1 is 0.35 times the electron mass at rest. Generally, a Lorentzian is theoretically derived for the functional form of the CR lines for homogeneous systems [3]. We assume that there are two contributions to the width: the homogeneous (intrinsic) width owing to phonon scattering and the inhomogeneous (extrinsic) width. When the inhomogeneous width dominates over the homogeneous width, the spectral lines follow Gaussian functions.

First, we examine the carrier-density dependence. Figure 2(a) compares the CR spectrum obtained with the maximum CW light intensity at 3.7 K and that obtained under pulsed excitation at an electron density approximately 10 times higher (Supplemental Material S3 [21]). The peak-to-peak width of the CWCR spectrum is approximately 1/3 that of the TRCR spectrum, which is affected by carrier-carrier scattering. Figure 2(b) shows the CWCR spectra measured by reducing the incident light intensity at 3.0 K. The linear dependence of the CR signal intensity, as plotted in the inset, indicates that the electron density varies linearly with the light intensity, down to 10^8 cm^{-3}. Meanwhile, the spectral shape is retained as a Gaussian function with a 0.73-mT half-width (dashed lines). This independence against the density indicates ineffective carrier-carrier scattering as a result of weak CW excitation, and the line shape implies the dominance of inhomogeneous broadening other than carrier-carrier scattering.

Second, we investigate the effects of temperature variation and microwave power. Figure 3(a) depicts the CWCR spectra obtained at various temperatures. With decreasing temperature, the spectra become narrower, and the positive- and negative-going peaks increase significantly in strength. Figure 3(b) compares the normalized spectra at 2.9, 5.5, and 8.0 K. The differential form of the Lorentzian function, as depicted by the red lines, matches well with the data at 8.0 K. However, the spectrum gradually deviates from the Lorentzian with decreasing temperature, indicating a transition to a Gaussian functional form, as presented by the black lines.

We further reduce the microwave power at the sample position by reducing the cavity quality factor Q [27] and

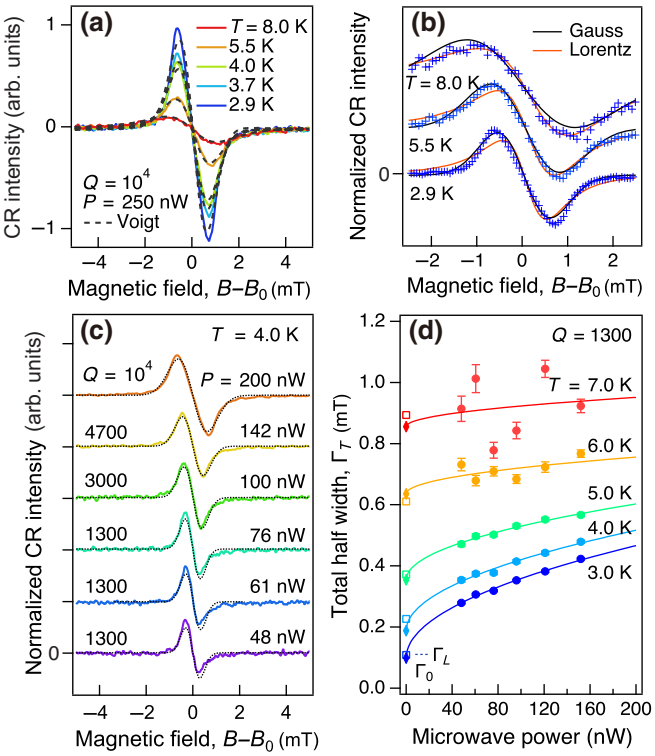

FIG. 3. (a) CWCR spectra measured in Sample 1 at different temperatures. Dashed lines represent fits by Eq. (1). (b) Normalized CWCR spectra with differential Lorentzian and Gaussian functions. (c) CWCR spectra measured in Sample 2 at various microwave powers P inside the cavity (corrected for the difference in Q). Dotted lines represent Gaussian fits. (d) Γ_T as a function of microwave power. Lines represent empirical fits assuming Eq. (2) with $\lambda = 0.5$.

adjusting the attenuator setting. A significant narrowing of the lines is observed at reduced microwave power at 4.0 K, as shown in Fig. 3(c). As the Gaussian component becomes dominant at this low temperature, fitting is performed using a Gaussian function. Here, the half width at half maximum (Γ_T) of the Gaussian is a fitting parameter that approximately includes both homogeneous and inhomogeneous broadening. Figure 3(d) shows Γ_T as a function of the microwave power P. At temperatures higher than 6.0 K, the width varies only slightly with the variation of P. Meanwhile, below 5.0 K, Γ_T substantially decreases with decreasing P. The temperature for the change of the line shape coincides with the temperature at which the width starts to sensitively change with P. This means that both these changes originate from inhomogeneous broadening owing to microwave power absorption [28].

A method for extracting homogeneous and inhomogeneous widths is yet to be established; therefore, we attempt two ways. Our ultimate goal is to extract an intrinsic scattering rate from fittings of different datasets and to check for internal consistency. For the temperature dependence measured at relatively high P [Figs. 3(a) and 3(b)], fitting is performed using a differential form of the Voigt function. The fitting function is expressed as

$$\frac{\partial}{\partial x}V(x) = \int G(y,\Gamma_G)\frac{\partial}{\partial x}L(x-y,\Gamma_L)dy, \qquad (1)$$

where $G(x,\Gamma_G) = (\sqrt{\ln 2}/\Gamma_G\sqrt{\pi})\exp[-x^2\ln 2/(\Gamma_G)^2]$ is a Gaussian function and $L(x,\Gamma_L) = (\Gamma_L\cos\theta + x\sin\theta)/\pi[x^2+(\Gamma_L)^2]$ is a Lorentzian function. θ includes the unintentional phase shift in the cavity, and $x = B - B_0$ is the difference in the magnetic field from the resonance. We globally fit the data by setting Γ_G and θ common for all temperatures. The best-fit functions are indicated by dashed lines in Fig. 3(a). We find that Γ_L decreases with decreasing temperature, down to 0.091 mT at 2.9 K with $\Gamma_G = 0.65$ mT and $\theta = -11^\circ$. The values of Γ_L for 3.0–7.0 K are marked by open squares at $P = 0$ in Fig. 3(d).

To investigate the P dependence [Figs. 3(c) and 3(d)], we assume that inhomogeneous broadening occurs proportionally to the power λ of P, that is, CP^λ, and fit the power dependence to

$$\Gamma_T(P) = \Gamma_0 + CP^\lambda, \qquad (2)$$

where Γ_0, C, and λ are adjustable parameters. The fitting with Eq. (2) [full lines in Fig. 3(d)] yields $\lambda \simeq 0.5$ and Γ_0 at each temperature, marked by the rhombuses in Fig. 3(d). Γ_0 corresponds to a homogeneous (Lorentzian) width, reflecting a scattering rate free from microwave power broadening. If there are no active scattering mechanisms other than acoustic phonon scattering, $1/\Gamma_0$ provides the intrinsic mobility.

The extracted Γ_L and Γ_0 values are in excellent agreement with each other for all measured temperatures, indicating that the assumptions in the two fitting methods are valid. It is noteworthy that although Γ_L (or Γ_0) is an important quantity, the Gaussian broadening from microwave power is dominant up to approximately 6 K, above which acoustic phonon scattering occurs strongly. Other broadening mechanisms, such as dislocation scattering [29], might appear at ultralow microwave powers (Supplemental Material S1 [21]). However, we obtain the same Γ_L values from samples with different dislocation densities, which implies that such an extrinsic effect is buried in the power broadening and effectively removed by our analyses.

The inset of Fig. 4 shows the spectrum with the smallest width, measured at 3.0 K and $P = 48$ nW. This spectrum, without any power-broadening correction and thereby free from any extrapolation or model-dependent fitting, already indicates an extraordinarily high mobility of $\mu_T = (\Gamma_T)^{-1} = 36\times10^6$ cm^2 V^{-1} s^{-1} (the triangle in Fig. 4). The slightly asymmetric line shape, owing to an unintentional phase shift, affects the evaluation of Γ_T

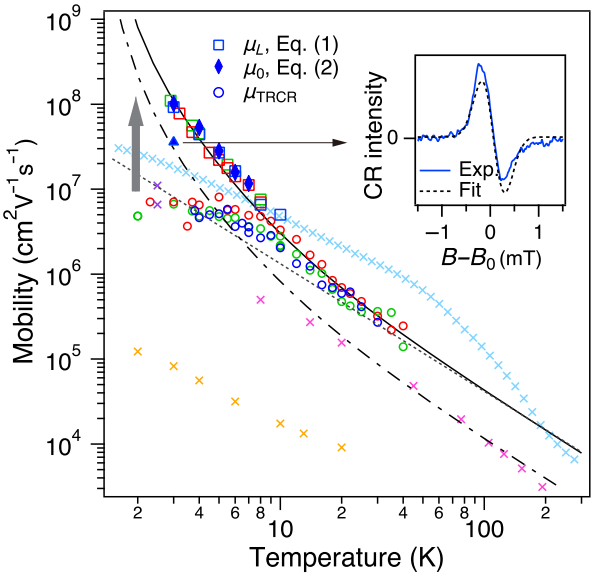

FIG. 4. Electron mobility as a function of temperature. Open squares, rhombuses, and circles represent mobility values from inverse Lorentzian widths, extrapolation to the zero microwave power limit, and TRCR [18], respectively. Green, blue, and red colors correspond to Samples 1, 2, and 3. Full and dotted lines represent calculations assuming inelastic and elastic acoustic-phonon scattering, while the dashed-dotted line shows TOF mobility [18]. Crosses represent mobility values measured in GaAs (cyan) and ZnO (orange) heterostructures by Hall effect [34,35] and those measured in bulk silicon by TOF (magenta) [36] and CWCR (purple) [23]. The inset shows a spectrum measured at 3.0 K, $P = 48$ nW, and $Q = 1300$, together with Gaussian fit (dotted line). The corresponding mobility value is indicated by the triangle.

within only 2%. The mobility values, $\mu_L = (\Gamma_L)^{-1}$ and $\mu_0 = (\Gamma_0)^{-1}$, are marked in Fig. 4 by open squares and rhombuses, respectively. These homogeneous widths indicate that the mobility values increase with decreasing temperature, reaching the value of 100×10^6 cm^2 V^{-1} s^{-1} at 3.0 K. As indicated by the upward arrow in Fig. 4, this goes beyond the limit imposed by the carrier-carrier scattering so far [18], and corresponds to a 16-fold improvement in the mobility, relative to the previous record in diamond (circles).

The theoretical mobility curve, considering the inelastic acoustic-phonon scattering of electrons, is depicted by the full line in Fig. 4 [14,30,31]. Good agreement is observed between the measured and calculated temperature dependences, demonstrating the enhanced mobility as compared with that of classical $T^{-3/2}$ dependence (dotted line). This enhancement is caused by the quenching of phonon scattering owing to the shift from elastic to inelastic scattering regimes. The threshold temperature for the full quantum CR regime [32,33], where other peculiar mechanisms such as inter-Landau-level scattering enter, is $\hbar(2\pi f)/k_B = 0.46$ K and is lower than the temperature range used in our experiments.

Finally, we provide a comment on a comparison with other material systems. The mobility determined by CR with small cyclotron radii of the order of 100 nm reflects the properties of the carriers confined in high-quality regions. Therefore, our local mobility by CR is approximately 3.7 times the nonlocal mobility by TOF measurements on the same samples (dashed-dotted line in Fig. 4) [18]. When this difference is considered, the mobility in diamond is similar to that in silicon (magenta crosses, measured by TOF) [23,36] in the elastic scattering regime but increases to significantly higher values in the inelastic scattering regime owing to the high sound velocity in diamond. Such enhancement is also known for excitons of large translational effective masses [37,38] while almost saturating Hall mobility is observed for electrons of small effective masses in III-V compound semiconductors (cyan crosses) [34]. Although a direct comparison is not straightforward because of the different measurement schemes, it is surprising that the local electron mobility in bulk diamond is close to the nonlocal mobility of ultrahigh-quality GaAs 2DEG, which demonstrates the ultrahigh mobility (44×10^6 cm^2 V^{-1} s^{-1}) at 0.3 K after the recent breakthrough [39] and the high-order fractional quantum Hall states. The Hall mobility of 2DEGs in wider-band-gap semiconductors, such as heteroepitaxial ZnO/MgZnO [35] and GaN/AlGaN [10], is improving but is still significantly lower, that is, in the range of 0.1×10^6 cm^2 V^{-1} s^{-1} at a few kelvins (orange crosses).

In summary, we observe an extremely narrow CR spectrum of low-density electrons in diamond that unambiguously demonstrates a mobility value of 36×10^6 cm^2 V^{-1} s^{-1}. After separating the microwave power broadening effect, we reveal the intrinsic mobility limit imposed purely by inelastic scattering by acoustic phonons. The extraction of the intrinsic mobility (with a 16-fold improvement) is not possible using our previous TRCR scheme or by conventional transport measurements; thus, we propose an advanced methodology for elucidating carrier transport in a wide-band-gap semiconductor. This study provides valuable information on low-temperature charge carriers, which are difficult to activate in diamond. This study thus has direct relevance to the design and interpretation of diamond radiation detectors used at cryogenic temperatures [19]. Our findings imply that the intrinsic mobility values can generally be reached under minimized perturbations of the carrier system and provide an insight to clarify the highest possible mobility values in semiconductors [40].

ACKNOWLEDGMENTS

Element Six Ltd is gratefully acknowledged for providing samples. This work is partially supported by

Japan Society for the Promotion of Science (JSPS) bilateral Project No. 120209919, JSPS KAKENHI Grants No. 17H02910, No. 19K21849, and No. 21K03420, and Swedish Research Council Grant No. 2018-04154.

[1] F. Staub, H. Hempel, J-Ch. Hebig, J. Mock, U. W. Paetzold, U. Rau, T. Unold, and T. Kirchartz, Beyond Bulk Lifetimes: Insights into Lead Halide Perovskite Films from Time-Resolved Photoluminescence, Phys. Rev. Appl. **6**, 044017 (2016).

[2] O. Gunawan, S. R. Pae, D. M. Bishop, Y. Virgus, J. H. Noh, N. J. Jeon, Y. S. Lee, X. Shao, T. Todorov, D. B. Mitzi, and B. Shin, Carrier-resolved photo-Hall effect, Nature **575**, 155 (2019).

[3] G. Dresselhaus, A. F. Kip, and C. Kittel, Cyclotron resonance of electrons and holes in silicon and germanium crystals, Phys. Rev. **98**, 368 (1955).

[4] A. Kriisa, R. L. Samaraweera, M. S. Heimbeck, H. O. Everitt, C. Reichl, W. Wegscheider, and R. G. Mani, Cyclotron resonance in the high mobility GaAs/AlGaAs 2D electron system over the microwave, mm-wave, and terahertz-bands, Sci. Rep. **9**, 2409 (2019).

[5] A. Baydin, T. Makihara, N. M. Peraca, and J. Kono, Time-domain terahertz spectroscopy in high magnetic fields, Front. Optoelectron. **14**, 110 (2020).

[6] D. Nakamura, H. Saito, H. Hibino, K. Asano, and S. Takeyama, Quantum limit cyclotron resonance in monolayer epitaxial graphene in magnetic fields up to 560 T: The relativistic electron and hole asymmetry, Phys. Rev. B **101**, 115420 (2020).

[7] T. Akiho and K. Muraki, Screening Effects of Superlattice Doping on the Mobility of GaAs Two-Dimensional Electron System Revealed by in Situ Gate Control, Phys. Rev. Appl. **15**, 024003 (2021).

[8] T. Maag, A. Bayer, S. Baierl, M. Hohenleutner, T. Korn, C. Schueller, D. Schuh, D. Bougeard, C. Lange, R. Huber, M. Mootz, J. E. Sipe, S. W. Koch, and M. Kira, Coherent cyclotron motion beyond Kohn's theorem, Nat. Phys. **12**, 119 (2016).

[9] B. Cheng, P. Taylor, P. Folkes, C. Rong, and N. P. Armitage, Magnetoterahertz Response and Faraday Rotation from Massive Dirac Fermions in the Topological Crystalline Insulator $Pb_{0.5}Sn_{0.5}Te$, Phys. Rev. Lett. **122**, 097401 (2019).

[10] A. Wolos and A. Drabinska, Application of microwave spectroscopy to studies of electron transport properties, J. Cryst. Growth **401**, 314 (2014).

[11] N. Naka, H. Morimoto, and I. Akimoto, Excitons and fundamental transport properties of diamond under photoinjection, Phys. Status Solidi A **213**, 2551 (2016).

[12] N. Naka, I. Akimoto, M. Shirai, and K. Kan'no, Time-resolved cyclotron resonance in cuprous oxide, Phys. Rev. B **85**, 035209 (2012).

[13] I. Akimoto and N. Naka, Two optical routes of cold carrier injection in silicon revealed by time-resolved excitation spectroscopy, Appl. Phys. Exp. **10**, 061301 (2017).

[14] I. Akimoto, K. Fukai, Y. Handa, and N. Naka, High carrier mobility in ultrapure diamond measured by time-resolved cyclotron resonance, Appl. Phys. Lett. **105**, 032102 (2014).

[15] T. Shimomura, Y. Kubo, J. Barjon, N. Tokuda, I. Akimoto, and N. Naka, Quantitative relevance of substitutional impurities to carrier dynamics in diamond, Phys. Rev. Mater. **2**, 094601 (2018).

[16] H. Kawamura, H. Saji, M. Fukai, K. Sekido, and I. Imai, Cyclotron resonance line broadening due to carrier-carrier interaction in germanium, J. Phys. Soc. Jpn. **19**, 288 (1964).

[17] N. Naka, K. Fukai, Y. Handa, and I. Akimoto, Direct measurement via cyclotron resonance of the carrier effective masses in pristine diamond, Phys. Rev. B **88**, 035205 (2013).

[18] K. Konishi, I. Akimoto, H. Matsuoka, V. Djurberg, S. Majdi, J. Isberg, and N. Naka, Low-temperature mobility-lifetime product in synthetic diamond, Appl. Phys. Lett. **117**, 212102 (2020).

[19] C. Kurfürst, B. Dehning, M. Sapinski, M. R. Bartosik, T. Eisel, C. Fabjan, C. A. Rementeria, E. Griesmayer, V. Eremin, E. Verbitskaya, A. Zabrodskii, N. Fadeeva, Y. Tuboltsev, I. Eremin, N. Egorov, J. Härkönen, P. Luukka, and E. Tuominen, In situ radiation test of silicon and diamond detectors operating in superfluid helium and developed for beam loss monitoring, Nucl. Instrum. Methods A **782**, 149 (2015).

[20] K. Konishi, I. Akimoto, J. Isberg, and N. Naka, Diffusion-related lifetime and quantum efficiency of excitons in diamond, Phys. Rev. B **102**, 195204 (2020).

[21] See Supplemental Material at http://link.aps.org/supplemental/10.1103/PhysRevApplied.17.L031001 for dislocation scattering, estimation of the electron density, and the carrier-carrier scattering effect observed by the TRCR method.

[22] K. Konishi and N. Naka, Phonon-assisted excitonic absorption in diamond, Phys. Rev. B **104**, 125204 (2021).

[23] H. Malissa, Z. Wilamowski, and W. Jantsch, Plasmon-cyclotron resonance in ultra-high mobility bulk silicon, AIP Conf. Proc. **1199**, 63 (2010).

[24] I. Akimoto, S. Torai, N. Naka, and M. Shirai, Temporal shift from magnetoplasma resonance to cyclotron resonance of photo carriers generated from 1s-exciton in cuprous oxide crystal, EuroPhys. J. B **85**, 374 (2012).

[25] D. K. Schroder, *Semiconductor Material and Device Characterization* (John Wiley & Sons, New York, 2015), 3rd ed.ISBN0471739065.

[26] We confirmed that further reduction in the modulation amplitude does not change the spectral shapes.

[27] Y. Ohba, C. Watanabe, S. Nakazawa, and S. Yamauchi, Determination of quality factor for highly overcoupled EPR resonators, Appl. Magn. Reson. **37**, 781 (2010).

[28] H. Malissa, Z. Wilamowski, and W. Jantsch, Cyclotron resonance revisited: The effect of carrier heating, AIP Conf. Proc. **772**, 1218 (2005).

[29] D. L. Dexter and F. Seitz, Effects of dislocations on mobilities in semiconductors, Phys. Rev. **86**, 964 (1952).

[30] S. Majdi, M. Gabrysch, K. K. Kovi, N. Suntornwipat, I. Friel, and J. Isberg, Low temperature conduction-band transport in diamond, Appl. Phys. Lett. **109**, 162106 (2016).

[31] We calculate the mobility considering inelastic scattering by longitudinal acoustic phonons using Eqs. (1)–(3) of Ref. [30]. The integration over κ is performed numerically and an isotropic effective deformation potential $D_A = 8.0$ eV is assumed.

[32] H. J. G. Meyer, On the low temperature limit of mm-wave cyclotron resonance line widths, Phys. Lett. **2**, 259 (1962).

[33] H. Kobori, T. Ohyama, and E. Otsuka, Line-width of quantum limit cyclotron resonance. I. Phonon scatterings in Ge, Si, CdS and InSb, J. Phys. Soc. Jpn. **59**, 2141 (1990).

[34] D. G. Schlom and L. N. Pfeiffer, Upward mobility rocks!, Nat. Mater. **9**, 881 (2010).

[35] J. Falson, Y. Kozuka, M. Uchida, J. H. Smet, T. Arima, A. Tsukazaki, and M. Kawasaki, MgZnO/ZnO heterostructures with electron mobility exceeding 1×10^6 cm^2/Vs, Sci. Rep. **6**, 26598 (2016).

[36] C. Canali, C. Jacoboni, F. Nava, G. Ottaviani, and A. A. Quaranta, Electron drift velocity in silicon, Phys. Rev. B **12**, 4 (1975).

[37] D. P. Trauernicht and J. P. Wolfe, Drift and diffusion of paraexcitons in Cu_2O, Phys. Rev. B **33**, 8506 (1986).

[38] H. Morimoto, Y. Hazama, K. Tanaka, and N. Naka, Ultrahigh exciton diffusion in intrinsic diamond, Phys. Rev. B **92**, 201202(R) (2015).

[39] Y. J. Chung, K. A. Villegas Rosales, K. W. Baldwin, P. T. Madathil, K. W. West, M. Shayegan, and L. N. Pfeiffer, Ultra-high-quality two-dimensional electron systems, Nat. Mater. **20**, 632 (2021).

[40] E. H. Hwang and S. Das Sarma, Limit to two-dimensional mobility in modulation-doped GaAs quantum structures: How to achieve a mobility of 100 million, Phys. Rev. B **77**, 235437 (2008).